RADBOUD UNIVERSITY

BSc PHYSICS AND ASTRONOMY

BACHELOR THESIS

Modelling Stochastic Dynamics using Quantum Boltzmann Machines

---

Author:
Jasper PIETERSE

Daily Supervisor:
Dr. E.J. DOMÍNGUEZ VÁZQUEZ

First Supervisor
Prof. Dr. H. J. KAPPEN

Second Supervisor:
Prof. Dr. A. C. C. COOLEN

Department of Neurophysics

Abstract

This bachelor thesis investigates how the parameters of a quantum Boltzmann machine (QBM) encode the properties of a binary stochastic dynamics. We describe a toy dynamics that allows control over its equilibrium and dynamical properties. Next, we describe a quantum-classical mapping, in which the toy dynamics is encoded in a density matrix, and learned by the QBM. Using the quantum-classical mapping, we demonstrate how the quantum parameters are related to equilibrium and dynamical properties of the dynamics. Notably, we establish a non-trivial connection between state-dependent transitions and a subset of quantum parameters.

Contents

1 Introduction

Machine learning (ML) is the process of enabling computer systems to learn from data by using algorithms and statistical models. Within ML, a fundamental research goal is to discover the statistical-computational laws that govern learning systems [1]. ML models are prominent throughout society, powering state-of-the-art recommendation systems [2], autonomous vehicle control [3] and image recognition systems [4]. Furthermore, ML models are becoming increasingly widespread within the physical sciences [5] with applications in, for example, neuroscience [6], quantum chemistry [7] and climate modelling [8].

Due to recent developments in quantum hardware [9], there is a growing interest in adapting ML algorithms to the quantum domain. Quantum algorithms can exploit quantum phenomena in their computation, which can lead to significant speedups and enhanced data analysis over their classical counterparts [10]. However, constructing quantum algorithms is challenging due to the non-commutative nature of quantum mechanics, and the limited amount of qubits on quantum hardware. As of date, there remain open questions regarding the efficiency, computational power, and utility of quantum ML algorithms [11].

One common challenge in ML is how to effectively learn the parameters of a statistical model from observed data [12]. Statistical models provide a mathematical description of how our data might be generated, allowing us to make sense of the data and generate new data once we know the model's parameters. However, inferring these parameters can be a complex task. In this context, the Boltzmann Machine (BM) has been developed as an algorithm to address this challenge.

The BM uses the Boltzmann distribution of statistical mechanics as a statistical model to effectively model and learn patterns of data. A BM represents data as a thermal state of an Ising model Hamiltonian [13]. This means that the parameters a BM learn physically correspond to the parameters of an Ising Hamiltonian [14]. While the BM has been foundational in the development of deep learning models like deep belief networks and deep Boltzmann Machines [15–17], they are not as commonly used today. This is primarily because training BMs can be computationally expensive and they have limited modelling capacity [18].

The quantum Boltzmann Machine (QBM) [19] is a quantum adaptation of the BM. The QBM represents data as a thermal state of a quantum Ising model Hamiltonian. The QBM can infer the parameters of a quantum Ising Hamiltonian by learning a density matrix. Learning this density matrix gives rise to quantum statistics that capture additional information beyond classical statistics.

Recently it has been shown that the QBM can directly learn classical data distributions represented in a density matrix. The quantum statistics inferred by the QBM capture properties of the classical data distribution that are otherwise inaccessible to a classical BM, allowing the QBM to learn *classical* problems better than a BM. In fact, for certain problems, the QBM's quantum features are necessary for

accurate modelling, indicating its ability to capture more information, including higher-order correlations [20].

In contrast, a classical BM can only access first and second-order correlations, allowing it to only learn the equilibrium properties of a system, without information about the dynamics that gave origin to it. We want to investigate if the QBM's ability to learn higher-order correlations means it can also capture dynamical properties of the system. Given that the QBM represents data as a thermal state of a quantum Ising Hamiltonian, it suggests that the parameters of the quantum equilibrium Hamiltonian may encode classical dynamical effects.

This thesis aims to analyse how the dynamical properties of a system are encoded by the quantum statistics of a QBM. To this end, we will define a toy binary stochastic dynamics for which we can vary both equilibrium and dynamical properties systematically. The binary stochastic dynamics describes how an ensemble of binary variables evolves probabilistically over time and can be effectively described using a Markov chain. The toy dynamics can be encoded in a density matrix. Using a QBM, we can learn this density matrix to infer the parameters of the quantum Ising Hamiltonian. We can then investigate how the properties of the stochastic dynamics map to the parameters of the QBM. We will refer to this mapping of parameters as the quantum-classical mapping.

There are two main motivations for studying the quantum-classical mapping. Firstly, it provides insight into how the QBM as a modelling tool enhances the analysis of binary stochastic dynamics. By understanding what information the parameters of a QBM encode about the dynamics, we can gain valuable insights for data analysis. Secondly, it provides insight into how the QBM outperforms the classical BM in specific tasks, showcasing the benefits of "quantizing" classical algorithms.

Binary stochastic dynamics find applications in various fields. In physics, Markov chain Monte Carlo methods can be used to simulate the stochastic dynamics of Ising models, allowing for exploration of their equilibrium distribution [21]. In neuroscience, modelling neural networks using stochastic dynamics allows for understanding the dynamics of information processing in the brain [22]. Furthermore, understanding the stochastic dynamics of artificial binary synapses can potentially aid in the development of energy-efficient neuromorphic hardware [23–25].

This thesis is structured as follows. The second chapter is centred around stochastic dynamics. We will describe a toy dynamics of which we can vary various equilibrium and dynamical properties. In the third chapter, we will introduce the Quantum Boltzmann machine. We will explain the quantum formalism of the QBM and demonstrate how it can infer the parameters of a quantum Ising Hamiltonian. The fourth chapter will focus on the quantum-classical mapping. Here we will describe the theory behind how we can map the parameters of a BM to the parameters of a QBM. We also highlight the methods used to perform the quantum-classical mapping. In the fifth chapter, we will present the results. We will discuss how the properties of the classical dynamics map to the parameters of the QBM. Finally, in the sixth chapter, we will discuss the results and conclude the thesis.

2 Stochastic Dynamics

In this chapter, we describe the toy dynamics that forms the basis for exploring the quantum-classical mapping. Our focus lies on a dynamics exhibiting both single and double-spin flips and satisfying the condition of detailed balance. Initially, we establish the formalism required to describe binary stochastic dynamics using a Markov chain. Subsequently, we introduce a parametrization that modulates that modulate biases, correlations, and timescales of the dynamics. Ultimately, we will explain how these classical parameters relate to the equilibrium and dynamical properties of the system.

2.1 Binary stochastic dynamics

A binary stochastic dynamics describes the probabilistic state-to-state evolution of an ensemble of binary variables over time. Stochastic dynamics naturally occur in dynamical systems that are subjected to the effects of noise [26]. More generally, they provide a framework for modelling and understanding the behaviour of systems influenced by random processes. In this work, we will refer to binary variables as spins, but the discussion remains applicable to any binary variable.

2.1.1 State space

A state of the system is represented as $s = (s_1, \ldots, s_N)$, where each spin possesses a binary and stochastic value denoted by $s_i = \pm 1$. Consequently, a system comprising N spins possesses 2^N possible states. The probability of the system being in a state s at time t is denoted as $p_t(s)$, while the time-independent transition rate from a state s to a state s' is denoted by $W(s'|s)$. A general description of the dynamics is defined through a master equation [21]:

$$\frac{dp_t(s)}{dt} = \sum_{s'} \left[W(s|s')p_t(s') - W(s'|s)p_t(s) \right] \tag{2.1}$$

In this equation, the first term on the right-hand side corresponds to the rate at which the system is transitioning into state s, while the second term corresponds to the rate at which the system is transitioning out of state s into states s'. This process is visualized in Figure 2.1(a). When using discretized time intervals Δt, the master equation can be written as:

$$p_{t+1}(s') = \sum_{s} W(s'|s)p_t(s) \tag{2.2}$$

We can simulate the state-to-state dynamics of our system using the transition matrix $W(s'|s)$.

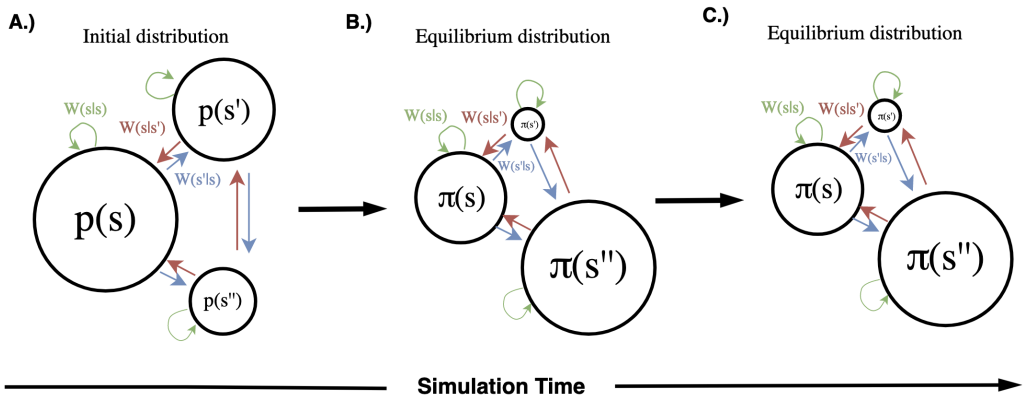

FIGURE 2.1: **Abstract visualization of the evolution of state space. A**, The size of the circles represents the probability of a state $p(s)$. The coloured arrows represent the transition rates. $\mathbf{A} - \mathbf{C}$, If a dynamics satisfies detailed balance, the initial distribution $\vec{p}$ eventually converges to the equilibrium distribution $\vec{\pi}$. Once converged, the probabilities remain static, though the system still undergoes dynamical changes [28].

2.1.2 Detailed balance

A dynamics has reached equilibrium once the state probabilities remain static over time [27]. This means the probability distribution $\vec{p}_t$ converges to the equilibrium distribution $\vec{\pi}$:

$$\lim_{t\to\infty} \vec{p}_t = \vec{\pi} \tag{2.3}$$

The equilibrium distribution $\vec{\pi}$ represents the probability of observing the spin system in a particular state once the system has reached thermal equilibrium. Once converged, the equilibrium occupation probabilities $\pi(s)$ remain static:

$$\sum_s W(s'|s)\pi(s) = \pi(s') \tag{2.4}$$

This condition has been visualized in Figure 2.1

To ensure the dynamics converges to the equilibrium distribution, it has to satisfy the condition of detailed balance for all states s [29]:

$$W(s'|s)\pi(s) = W(s|s')\pi(s') \tag{2.5}$$

The left-hand side of the equation can be interpreted as the probability current flowing out of state s. The right-hand side can be interpreted as the probability current flowing out of state s'. The condition of detailed balance then states that the net probability current of all states is equal to zero.

2.1.3 Markov chains

A first-order homogenous Markov process is a mechanism that given a state s generates a new state s'. This process has to satisfy two properties: (1) The probability for the new state only depends on the current state and is given by a static transition matrix $W(s'|s)$. This is called the Markov property. (2) The Markov chain always has to transition to some state [30]:

$$\sum_{s'} W(s'|s) = 1 \tag{2.6}$$

A first-order homogenous Markov process can be used to generate a set of sequential samples from a system:

$$s \mapsto s' \mapsto s'' \mapsto \dots$$

We call this set of samples the Markov chain [31]. The Markov chain itself has to satisfy the condition of ergodicity. This means that all states within the allowed energy range in phase space can be reached by the Markov chain.

2.2 Toy dynamics

We use a transition matrix $W(s'|s)$ to define a discrete-time homogenous toy dynamics. $W(s'|s)$ is a non-negative left stochastic matrix whose entries describe the probability of transitioning from state s to state s'. We will use the following parametrization of the transition matrix:

$$W(s'|s) = W(s|s)\delta_{s',s} + \sum_i g_i(s)\delta_{s',F_i[s]} + \sum_{ij} g_{ij}(s)\delta_{s',F_{ij}[s]} \tag{2.7}$$

In this expression, g_i and g_{ij} represent the probabilities of single and double-spin flips respectively. The flip operator $F_a[\ ]$ flips a subset a spins, chosen from the N spins within a particular state s. The self-transitions $W(s|s)$ are defined as $1 - \sum_{s'} W(s|s')$. The flip probabilities $g_i(s)$ and $g_{ij}(s)$ establish the normalization of the self-transitions and should be parametrized such that $W(s|s) > 0$. The flip probabilities are defined as follows:

$$g_i(s) = \exp\left(-w_{s,F_i[s]} - s_i\left[h_i + \sum_{i\neq j} J_{ij}s_j\right]\right) \tag{2.8}$$

$$g_{ij}(s) = \exp\left(-w_{s,F_{ij}[s]} + J_{ij}s_is_j - s_i\left[\sum_i J_{ik}s_k + h_i\right] - s_j\left[\sum_{i'} J_{jk'}s_{k'} + h_j\right]\right) \tag{2.9}$$

In this formulation, J_{ij} represents the coupling strength between spins i and j, while h_i corresponds to the local field acting on spin i. These parameters have similar roles as the parameters in an Ising model (as discussed in Appendix A). The parameter w_{s,F_as} controls the timescale of spin flips involving the spin(s) a. Increasing $w_{s,F_i[s]}$ reduces the flipping rate of spin i, while increasing $w_{s,F_{ij}[s]}$ decreases the double-spin flip rate of spins i and j.

The equilibrium distribution of the transition matrix can be expressed as:

$$\vec{\pi} = \frac{1}{Z}e^{\sum_{\langle ij\rangle} J_{ij}s_is_j + \sum_i h_is_i} \tag{2.10}$$

Where Z is the partition function given by:

$$Z = \sum_s e^{\sum_{\langle ij\rangle} J_{ij}s_is_j + \sum_i h_is_i} \tag{2.11}$$

Where $\langle ij \rangle$ denotes the sum over all pairs i and j. The parameters J_{ij} and h_i are equilibrium parameters that offer insights into the long-term average behaviour of the system. It is worth noting that even when the dynamics reaches a steady state, it can still display dynamic effects.

2.2.1 Enforcing detailed balance

For our toy dynamics to converge to the equilibrium distribution, we have to satisfy the condition of detailed balance. We can enforce the condition of detailed balance as follows. We rewrite the condition of detailed balance (2.5) as:

$$\frac{W\left(F_a(s)|s\right)}{W\left(s|F_a(s)\right)} = \frac{\pi\left(F_a(s)\right)}{\pi(s)} \tag{2.12}$$

which can be further simplified to:

$$\frac{g_a(s)}{g_a\left(F_a(s)\right)} = \frac{\pi\left(F_a(s)\right)}{\pi(s)} \tag{2.13}$$

From this follows, that to satisfy detailed balance, the timescale parameters and the interaction strengths should be chosen symmetric: $w_{s,s'} = w_{s',s}$ and $J_{ij} = J_{ji}$. Note that the symmetry of J_{ij} is with respect to the spins, while the symmetry of $w_{s,s'}$ is with respect to the states.

2.2.2 State dependent transition rates

The benefit of defining the toy dynamics in (2.8) and (2.9) is the ability to control various dynamical properties by manipulating $w_{s,s'}$, without affecting the equilibrium distribution. This level of control is not possible using conventional 1-spin flip dynamics, such as Glauber dynamics [32]. However, the requirement of symmetry imposes constraints on the dependence of $w_{s,s'}$ on the states s and s'.

In general, the transition rate can depend on any n-order term. We have chosen to work with 2-body interactions because the toy dynamics, as defined in (2.8) and (2.9), incorporates up to 2-body interactions through J_{ij}. We do not anticipate the need for higher-order correlations in the rates. The general parametrization for a 2-body state-dependent transition rate is given by:

$$w_{s,F_a[s]} = b_a^0 + \sum_i b_i s_i + \sum_{\langle i,j \rangle} b_{ij} s_i s_j \tag{2.14}$$

We use the notation $s' = F_a[s]$ to indicate that the transition rate depends only on the initial state s and the spins a that are being flipped during the transition. Using this expression, the symmetry condition $w_{s,F_a[s]} = w_{F_a[s],s}$ can be expanded as follows:

$$\sum_i b_i s_i + \sum_{\langle i,j \rangle} b_{ij} s_i s_j = \sum_i b_i F_a[s_i] + \sum_{\langle i,j \rangle} b_{ij} F_a[s_i s_j] \tag{2.15}$$

To satisfy symmetry, only the terms that are invariant under the flip operator $F_a[\,]$ can have a non-zero value. For single-spin flip transitions, this leads to the following expression:

$$w_{s,F_i[s]} = b_i^0 + \sum_k b_k s_k + \sum_{\langle k,l \rangle} b_{kl} s_k s_l \tag{2.16}$$

Similarly, for double-spin flip transitions, the transition rate can be expressed as:

$$w_{s,F_{ij}[s]} = b_{ij}^0 + \sum_k b_k s_k + b_{ij} s_i s_j + \sum_{\langle k,l \rangle} b_{kl} s_i s_j \tag{2.17}$$

where $\langle k, l \rangle$ refers to summation over pairs $k, l \neq i, j$. Interpreting these in terms of flipping rates, we see that the rate of a single-spin flip s_i can depend on any spin s_j where $j \neq i$, as well as the product of spins that are not flipping $s_j s_k$. Similarly, the rate of a double-spin flip involving spins s_i and s_j can depend on any spin s_k where $s_k \neq s_i, s_j$, the product of spins that are not flipping $s_j s_k$, and the product of spins that are flipping $s_i s_j$.

3 The Quantum Boltzmann Machine

The Boltzmann machine (BM) can determine the equilibrium parameters h_i and J_{ij} of a binary stochastic dynamics (explained in Appendix A). However, it lacks the ability to infer dynamic effects such as spin flipping rates or state-dependent flipping rates. This chapter introduces the Quantum Boltzmann Machine (QBM) [19], which extends the BM to the quantum domain. The QBM can learn the Hamiltonian of a quantum system, where the Hamiltonian parameters can encode dynamic effects. We first describe the quantum formalism needed to describe the QBM, followed by the definition of the QBM and its learning procedure.

3.1 Quantum formalism

One key difference between the QBM and the BM is how they represent spins. In the QBM, binary spins are described using Pauli spin matrices. In each measurement, the states of the qubits are read out in the sigma-z basis and the outcome will be a classical value ± 1, maintaining the ability of the system to describe binary variables.

3.1.1 Pauli spin operators

In the σ^z basis, the Pauli spin matrices are defined as:

$$\hat{\sigma}^x = \begin{bmatrix} 0 & 1 \\ 1 & 0 \end{bmatrix} \quad \hat{\sigma}^y = \begin{bmatrix} 0 & -i \\ i & 0 \end{bmatrix} \quad \hat{\sigma}^z = \begin{bmatrix} 1 & 0 \\ 0 & -1 \end{bmatrix} \tag{3.1}$$

The eigenvectors of $\hat{\sigma}^z$ are denoted as $|s_i = \pm 1\rangle$ with eigenvalues $s_i = \pm 1$. The Pauli spin matrices can act as operators on the individual spins:

$$\hat{\sigma}_i^x |s_i\rangle = |-s_i\rangle \qquad \hat{\sigma}_i^y |s_i\rangle = i s_i |-s_i\rangle \qquad \hat{\sigma}_i^z |s_i\rangle = s_i |s_i\rangle \tag{3.2}$$

The basis of the Hilbert space is a tensor product of the basis vectors $|s_i = \pm 1\rangle$ denoted as $|s\rangle = |s_1\rangle \otimes |s_2\rangle \otimes \cdots \otimes |s_N\rangle = |s_1, \ldots, s_N\rangle$. In this basis, the Hamiltonian becomes an operator with a dimension equal to the square of the number of possible states 2^N x 2^N.

3.1.2 Pauli terms

Pauli terms, also known as interaction matrices, represent different types of interactions between spins in the system. These terms can include single-spin interactions (such as $\hat{\sigma}_i^z$) or multi-spin interactions (such as $\hat{\sigma}_i^x \hat{\sigma}_j^y$). Generally, the Hamiltonian is composed of weighted sums of Pauli terms and encodes the properties of the quantum system.

The Hilbert space of an N-particle system is the tensor product of the single-particle Hilbert spaces. For consistent operations, all Pauli terms should be expressed in the same basis:

$$\hat{\sigma}_a^z \equiv \overbrace{\hat{I} \otimes \cdots \otimes \hat{I}}^{a-1} \otimes \hat{\sigma}_z \otimes \overbrace{\hat{I} \otimes \cdots \otimes \hat{I}}^{N-a}$$

In the following treatment, we will omit the explicit tensor products with the identity elements from our notation.

3.1.3 Density matrices

The density matrix $\hat{\rho}$ is a generalized representation of the state vector in quantum mechanics. Unlike the state vector, which describes pure states, the density matrix can also describe mixed states. In a sense, the density matrix can be seen as the quantum counterpart of a classical probability distribution $p(s)$.

The density matrix of a quantum system can be obtained by taking the matrix exponential of the Hamiltonian:

$$\hat{\rho} = \frac{e^{\hat{H}}}{Z} \tag{3.3}$$

with the partition function Z given by:

$$Z = \mathrm{Tr}\left[e^{\hat{H}}\right] \tag{3.4}$$

Here, $\hat{\rho}$ is a positive semi-definite Hermitian matrix with dimension 2^N x 2^N. The inverse temperature β is absorbed into the parameters of the Hamiltonian.

In practice, the density matrix can be obtained using the eigendecomposition of the quantum Hamiltonian:

$$\hat{\rho} = \sum_i p_i \left|s_i\right\rangle \left\langle s_i\right| \tag{3.5}$$

$\left|s_i\right\rangle \left\langle s_j\right|$ represents the projection operator associated with the basis states $\left|s_i\right\rangle$ and $\left|s_j\right\rangle$. The entries ρ_{ij} of the density matrix correspond to the probability amplitudes associated with the quantum state $\left|s_i\right\rangle \left\langle s_j\right|$.

The diagonal entries of the density matrix, ρ_{ii}, represent the probabilities of the system being in pure states $\left|s_i\right\rangle$. These probabilities should be non-negative and normalized, with the sum of all diagonal entries equal to one i.e., $\mathrm{Tr}[\hat{\rho}] = 1$. The off-diagonal entries ρ_{ij} with $i \neq j$, represent the probabilities associated with mixed states. They correspond to the coherences that describe superpositions between different quantum states.

The density matrix can be used to calculate the expectation value of any Hermitian operator $\hat{A}$ representing an observable, denoted as $\left\langle \hat{A} \right\rangle_\rho$. This is done by taking the trace of the matrix product of $\hat{A}$ and $\hat{\rho}$:

$$\left\langle \hat{A} \right\rangle_\rho = \mathrm{Tr}\left[\hat{A}\hat{\rho}\right] \tag{3.6}$$

3.2 Quantum Boltzmann machines

The QBM is defined as the N-qubit density matrix obtained from the quantum Boltzmann distribution (3.3). The QBM is capable of representing any general linear Hamiltonian:

$$\hat{H} = \sum_r w_r \hat{H}_r \tag{3.7}$$

where $\hat{H}$ and $\hat{H}_r$ are Hermitian matrices obtained from the Pauli terms and w_r is a real-valued parameter [33]. In this thesis, we chose to work with the most general form of a Hamiltonian with three-body interactions:

$$\hat{H} = \sum_{ijl} \sum_{k,k',k''} \sigma_{ijl}^{k,k',k''} \hat{\sigma}_i^k \hat{\sigma}_j^{k'} \hat{\sigma}_l^{k''} + \sum_{ij} \sum_{k,k} J_{ij}^{k,k'} \hat{\sigma}_i^k \hat{\sigma}_j^{k'} + \sum_i \sum_k h_i^k \hat{\sigma}_i^k \tag{3.8}$$

Here, the index $k = x, y, z$ refers to the summation over the Pauli spin orientations. The terms $\hat{\sigma}_i^k$, $\hat{\sigma}_j^{k'}$ and $\hat{\sigma}_l^{k''}$ denote the Pauli spin matrices acting on the spins at sites i, j and l, respectively. The coefficients $\sigma_{ijl}^{k,k',k''}$ encode the three-body interaction between the three spins at sites i, j, and l in the respective orientations k, k', and k''. $J_{ij}^{k,k'}$ represents the coupling strengths between spins at sites i and j in different orientations k and k'. The coefficients h_i^k represent the local magnetic fields at site i in the orientation k.

3.2.1 Learning Procedure

We can use a QBM to learn the quantum parameters of a model density matrix $\hat{\rho}$ that best matches the data density matrix $\hat{\eta}$. The learning process (also, training process) involves adjusting the weights of the Pauli terms to correctly capture the statistical dependencies in the observed data. The objective is to maximize the quantum likelihood function given by:

$$L = \mathrm{Tr}[\hat{\eta} \ln \hat{\rho}] \tag{3.9}$$

The learning rules for the QBM are derived by performing gradient ascent on this likelihood function. The learning rules for the Hamiltonian (3.8) are given by:

$$\Delta h_i^k = \epsilon \frac{\partial L}{\partial h_i^k} = \epsilon \left(\langle \hat{\sigma}_i^k \rangle_{\hat{\eta}} - \langle \hat{\sigma}_i^k \rangle_{\hat{\rho}} \right) \qquad \Delta J_{ij}^{kk'} = \epsilon \frac{\partial L}{\partial J_{ij}^{kk'}} = \epsilon \left(\langle \hat{\sigma}_i^k \hat{\sigma}_j^{k'} \rangle_{\hat{\eta}} - \langle \hat{\sigma}_i^k \hat{\sigma}_j^{k'} \rangle_{\hat{\rho}} \right)$$

$$\Delta \sigma_{ijl}^{kk'k''} = \epsilon \frac{\partial L}{\partial \sigma_{ijl}^{kk'k''}} = \epsilon \left(\langle \hat{\sigma}_i^k \hat{\sigma}_j^{k'} \hat{\sigma}_l^{k''} \rangle_{\hat{\eta}} - \langle \hat{\sigma}_i^k \hat{\sigma}_j^{k'} \hat{\sigma}_l^{k''} \rangle_{\hat{\rho}} \right) \tag{3.10}$$

Here, ϵ represents the learning rate, $\langle \hat{\sigma}_i^k \rangle_{\hat{\eta}}$, $\langle \hat{\sigma}_i^k \hat{\sigma}_j^k \rangle_{\hat{\eta}}$ and $\langle \hat{\sigma}_i^k \hat{\sigma}_j^{k'} \hat{\sigma}_l^{k''} \rangle_{\hat{\eta}}$ are the clamped expectation values computed from the data density matrix. $\langle \hat{\sigma}_i^k \rangle_{\hat{\rho}}$, $\langle \hat{\sigma}_i^k \hat{\sigma}_j^k \rangle_{\hat{\rho}}$ and $\langle \hat{\sigma}_i^k \hat{\sigma}_j^{k'} \hat{\sigma}_l^{k''} \rangle_{\hat{\rho}}$ are the model expectation values. For a full derivation of these learning rules, please refer to [20].

Algorithm 1: Quantum Boltzmann Machine Learning Algorithm

Data: Input data set
Result: Trained Quantum Boltzmann machine
Compute the data density matrix from the data, store as $\hat{\eta}$;
Compute the clamped expectation values from the data density matrix, store as $\langle \hat{\sigma}_i^k \rangle_{\hat{\eta}}$, $\langle \hat{\sigma}_i^k \hat{\sigma}_j^{k'} \rangle_{\hat{\eta}}$ and $\langle \hat{\sigma}_i^k \hat{\sigma}_j^{k'} \hat{\sigma}_l^{k''} \rangle_{\hat{\eta}}$;
Initialize the model weights of the QBM, store as w_{model};
while *the stopping criterion is not met* **do**
    Compute the model density matrix from w_{model}, store as $\hat{\rho}$;
    Compute the model expectation values, store as $\langle \hat{\sigma}_i^k \rangle_{\hat{\rho}}$, $\langle \hat{\sigma}_i^k \hat{\sigma}_j^{k'} \rangle_{\hat{\rho}}$ and $\langle \hat{\sigma}_i^k \hat{\sigma}_j^{k'} \hat{\sigma}_l^{k''} \rangle_{\hat{\rho}}$;
    Update the model weights w_{model} based on the learning rules;
end

The learning procedure for the QBM is summarized in Algorithm 1. It begins by computing the data density matrix $\hat{\eta}$ from the input data set and computing the clamped expectation values $\langle \hat{\sigma}_i^k \rangle_{\hat{\eta}}$, $\langle \hat{\sigma}_i^k \hat{\sigma}_j^{k'} \rangle_{\hat{\eta}}$ and $\langle \hat{\sigma}_i^k \hat{\sigma}_j^{k'} \hat{\sigma}_l^{k''} \rangle_{\hat{\eta}}$ using equation (3.6). Next, the quantum parameters of the model density matrix are initialized randomly. The algorithm then iteratively updates the model density matrix $\hat{\rho}$ using the current quantum parameters. From the model density matrix, it computes the free statistics $\langle \hat{\sigma}_i^k \rangle_{\hat{\rho}}$, $\langle \hat{\sigma}_i^k \hat{\sigma}_j^{k'} \rangle_{\hat{\rho}}$ and $\langle \hat{\sigma}_i^k \hat{\sigma}_j^{k'} \hat{\sigma}_l^{k''} \rangle_{\hat{\rho}}$ and updates the weights based on the learning rules. This process continues until the stopping criterion is met, indicating that the learning has converged.

4 Quantum-classical Mapping

This chapter explores the relationship between binary stochastic dynamics and the parameters of a Quantum Boltzmann Machine (QBM), which we will refer to as the 'quantum-classical mapping'. Our goal is to understand what information a QBM can gather about stochastic dynamics. First, we explain how classical data can be represented using a density matrix. Then, we analyse the quantum statistics that the QBM can deduce from binary stochastic dynamics and what they mean. Then we will describe different methods to analyse the quantum-classical mapping. These methods can give us insight into what information a QBM can learn and help explain why a QBM can outperform a classical Boltzmann Machine (BM) in specific problems.

4.1 Encoding classical data

To analyse classical dynamics using quantum models, we can encode the classical dynamics into a density matrix. Given a classical dynamics $W(s|s')$ and its steady-state distribution $q(s)$, we can construct density matrix using the following procedure:

$$A(s,s') \equiv \frac{1}{\sqrt{q(s)}} W(s|s') \sqrt{q(s')} \tag{4.1}$$

The steady-state distribution $q(s)$ of $W(s|s')$ can be obtained as the eigenvector corresponding to the largest eigenvalue $\lambda_{max} = 1$ of $W(s|s')$.

For the matrix A to be a valid density matrix, it needs to be Hermitian and positive semi-definite. Hermiticity is achieved when the dynamics satisfy detailed balance, making $W(s|s')$ symmetric. As a result, the matrix A will also be symmetric and have the same eigenvalues as $W(s|s')$ because (4.1) is a similarity transformation.

To ensure positive semi-definiteness, we increase the diagonal elements of $W(s|s')$. Using that $W(s|s) = 1 - \sum_s W(s|s')$, we can increase the diagonal by reducing the off-diagonal elements. This is done by scaling all $w_{s,s'}$ equally until the resulting eigenvalues are positive. Importantly, this procedure only affects the global timescale of the dynamics and doesn't change the equilibrium distribution or transition probability ratios.

Then we normalize the matrix to obtain the desired density matrix η:

$$\hat{\eta} = \frac{\hat{A}}{\mathrm{Tr}[\hat{A}]} \tag{4.2}$$

The resulting density matrix, $\hat{\eta}$, can be learned using a QBM.

4.2 Methods

4.2.1 Forward mapping

In the forward mapping method, we start with classical parameters represented by w, J, and h. Using equation (2.7), we calculate the transition matrix $W(s|s')$ that describes the dynamics of the classical system. This transition matrix is then transformed into a density matrix $\hat{\rho}$, which becomes the input for the QBM. The QBM then learns the quantum parameters that correspond to the classical system. The steps in this approach can be summarized as follows:

$$\begin{array}{ccccccc} \text{Classical Parameters} & & \text{Transition Matrix} & & \text{Density Matrix} & & \text{Quantum Parameters} \\ (w, J, h) & \rightarrow & W(s'|s) & \rightarrow & \hat{\rho} & \rightarrow & h^k, J^k, \sigma^k \end{array} \tag{4.3}$$

4.2.2 Inverse mapping

In the inverse mapping, we convert a quantum Hamiltonian to a density matrix and a density matrix to a transition matrix. Simulating this transition matrix allows us to generate a Markov chain. This Markov chain represents the stochastic dynamics of the system. This process can be summarized as follows:

$$\begin{array}{ccccccc} \text{Quantum Parameters} & & \text{Density Matrix} & & \text{Transition Matrix} & & \text{Markov chain} \\ (w, J, h) & \rightarrow & \hat{\rho} & \rightarrow & W(s'|s) & \rightarrow & (s, s', s'', \dots) \end{array} \tag{4.4}$$

4.2.3 Conditions for the quantum parameters

The off-diagonal elements of the density matrix can be complex and may have negative real or imaginary parts. However, negative elements in the density matrix lead to unphysical negative elements in the transition matrix W. To ensure the density matrix remains positive, we establish conditions for the quantum parameters that prevent the density matrix from becoming negative.

Since $\rho = e^{\hat{H}} \approx 1 + \hat{H} + \frac{\hat{H}^2}{2!} + \dots$, a sufficient (but not necessarily necessary) condition for a positive-valued ρ is that each off-diagonal component of $\hat{H}$ is positive. To determine these conditions, we collect Pauli terms with the same non-zero entries and ensure their sum is positive. For 2-body interactions, the following rules can be derived:

$$J_{ij}^{xx} > J_{ij}^{yy} \quad \text{for all} \quad i, j \tag{4.5}$$

$$h_i^x > \sum_{j \neq i} J_{ij}^{xz} \quad \text{for all} \quad i, j \tag{4.6}$$

When considering 3-body interactions, there are additional rules. However, for the purpose of this work, the only relevant rule is given by:

$$h_i^x > \sum_{j \neq i} J_{ij}^{xz} + \sum_{\langle jk \rangle} \sigma_{ijk}^{xzz} \quad \text{for all} \quad i, j, k \tag{4.7}$$

where $\langle jk \rangle$ denotes summation over all pairs $j, k \neq i$.

By following these conditions for the quantum parameters when performing the inverse mapping, we can ensure that the density matrix remains positive and physically meaningful in the quantum system.

5 Results

This chapter presents the findings obtained from the analysis of the binary stochastic dynamics of 2 and 3-spin systems and their relationship to the quantum parameters of the QBM. To establish this connection, we use the toy dynamics defined in equations (2.8) and (2.9) and apply the forward mapping technique explained in the previous chapter. Specifically, we employ a 2-body QBM Hamiltonian for the 2-spin systems and a 3-body QBM Hamiltonian for the 3-spin systems, as outlined in Chapter 3.

The objective is to perform a parameter sweep for specific configurations of the toy dynamics. In this sweep, we vary one or more classical parameters of the toy dynamics within a selected range, while keeping the other parameters fixed. For each plot, we divide the chosen range into 100 equidistant points. At each of these points, we perform a forward mapping from classical to quantum parameters. We then plot the values of the quantum parameters that have changed over the range of the parameter sweep. In these plots, we can see which quantum parameters are sensitive to changes in the classical parameters.

It is important to note that for all plots, when a classical parameter J_{ij} or $w_{s,s'}$ is varied, its symmetric counterpart is also varied equally to ensure detailed balance. Equally important to note is that for all the plots, the absence of a parameter does not necessarily imply a value of zero. Rather, it indicates that the parameter did not change significantly over the parameter sweep.

Furthermore, we employ an inverse mapping, in which we map a quantum Hamiltonian to a classical transition matrix. From this transition matrix, we derive a Markov chain, and we plot its time traces to visualize the inverse mapping. In these plots, the binary states {-1,1} are mapped to {0,1}. The states are numbered such that the state with all 0s is labelled as 1, and the leftmost bit is considered the most significant. For example, for a 2-bit system, the state order is as follows: State 1 represents (00), state 2 represents (01), state 3 represents (10), and state 4 represents (11). For the code used to generate these figures and additional implementation details, please refer to the GitHub repository [34].

5.1 Equilibrium parameters

We begin by analysing the correspondence between the classical equilibrium parameters h_i and J_{ij} and their quantum counterparts. We expect the h_1^z and J_{12}^{zz} terms of the QBM to encode the equilibrium parameters, as these terms map to the diagonal entries of the density matrix. The diagonal entries of the density matrix correspond to classical statistics that encode equilibrium properties.

Figure 5.1 shows the relationship between classical equilibrium parameters (h_1 and J_{12}) and their corresponding quantum parameters (h_1^z and J_{12}^{zz}) in a 2-spin system homogenous system. The left plot shows a parameter sweep over the classical

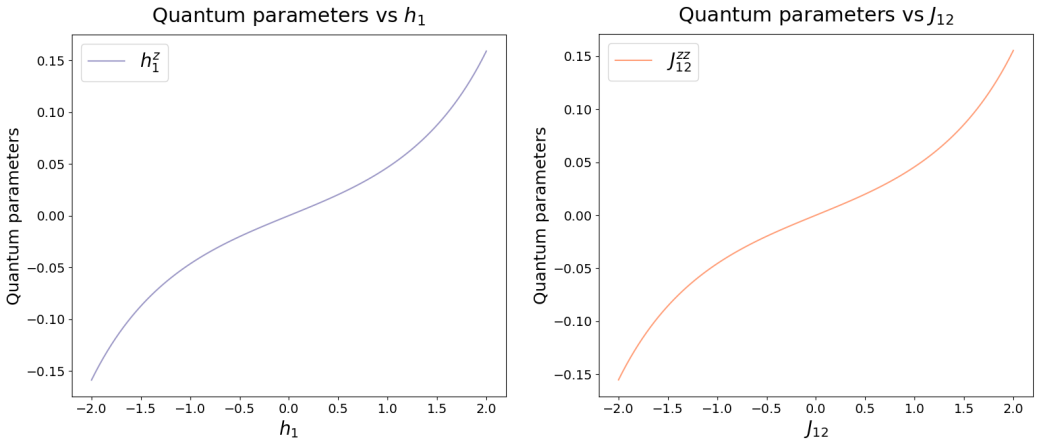

FIGURE 5.1: Relationship between classical equilibrium parameters (h_1 and J_{12}) and their corresponding quantum parameters (h_1^z and J_{12}^{zz}) in a homogenous 2-spin system. Left: Parameter sweep over the classical bias h_1 ($J_{12} = 0$, $h_2 = 0$, $w_{s,s'} = 4$). Right: Parameter sweep over the classical coupling J_{12} ($h_i = 0$, $w_{s,s'} = 4$).

bias h_1 in a non-interacting system ($J_{12} = 0$, $h_2 = 0$) with uniform transition rates ($w_{s,s'} = 4$). The right plot shows a parameter sweep over the classical coupling J_{12} in a system without biases ($h_i = 0$) with uniform transition rates ($w_{s,s'} = 4$).

In the left plot, we observe that when a non-zero bias h_1 is introduced, the corresponding quantum parameter h_1^z changes accordingly. The other quantum parameters remain unchanged. Furthermore, when performing the same parameter sweep for a connected system ($J_{12} \neq 0$, $h_2 \neq 0$), we also observe changes in the h_2^z parameter as h_1 varies. The magnitude of the change in h_2^z is proportional to the value of J_{12}.

In the right plot, introducing a non-zero coupling J_{12} leads to a corresponding change in the quantum parameter J_{12}^{zz}. The other quantum parameters remain unchanged. Similarly, when performing the same parameter sweep for a system with non-zero biases ($h_i \neq 0$), we observe changes in both h_1^z and h_2^z as we vary J_{12}, while the other quantum parameters remain unchanged. The magnitude of the change in h_1^z and h_2^z is proportional to the value of h_1 and h_2, respectively.

Based on these observations, we can conclude that the quantum parameters h_i^z and J_{ij}^{zz} play a similar role to their classical counterparts h_i and J_{ij} in encoding the equilibrium properties of the system. Furthermore, we conclude that in interacting systems, there is a mixture of effects, indicating the absence of a one-to-one correspondence between classical parameters and quantum parameters.

5.2 State-independent flipping rates

We now shift our focus to studying dynamical effects in the system. In Chapter 2, we introduced a parametrization for the state-dependent transition rates, given by the expressions (2.17) and (2.16). In this section, we are particularly interested in the constant term b_a^0, which solely depends on the flipped spin(s) a and is independent of the system's current state. Our goal is to determine if there is a corresponding quantum parameter for this term.

We can find a correspondence to b_i^0 by considering all transitions involving the flipping of s_i. Since varying all these transitions as a whole cancels out any dependence on the other states, we can establish a direct correspondence with b_i^0. Likewise, we can find a correspondence to b_{ij}^0 by considering all transitions involving the flipping of s_i and s_j. It is important to note that a higher value of $w_{s,s'}$ is associated with a longer timescale for that particular transition. In other words, a smaller $w_{s,s'}$ value corresponds to a higher rate for that transition.

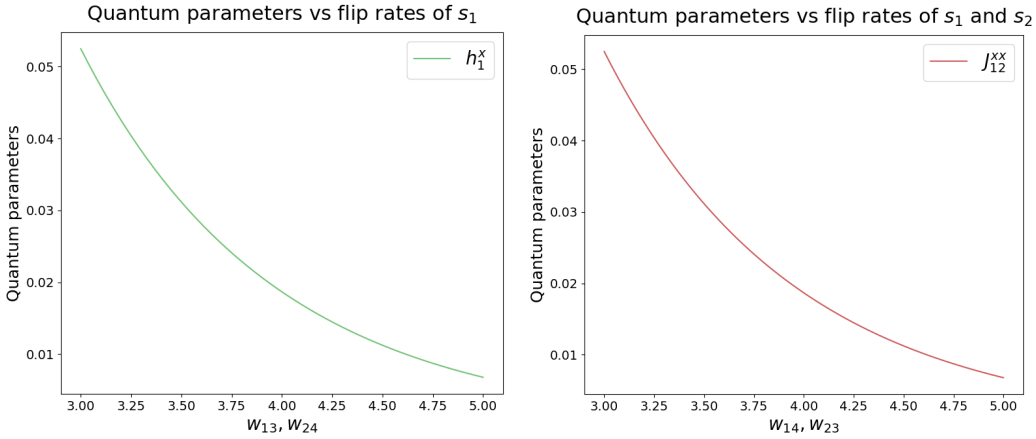

FIGURE 5.2: Relationship between state-independent flipping rates and their corresponding quantum parameters in a 2-spin system. Left: Parameter sweep over all transitions involving spin 1 flipping ($w_{s,F_1[s]}$) the other parameters are set as ($J_{12} = 0$, $h_i = 0$, $w_{s,F_2[s]} = 20$, $w_{s,F_{12}[s]} = 20$). Right: Parameter sweep over all transitions involving spin 1 and 2 flipping ($w_{s,F_{12}[s]}$) the other parameters are set as ($J_{12} = 0$, $h_i = 0$, $w_{s,F_1[s]} = 20$, $w_{s,F_2[s]} = 20$)

Figure 5.2 shows the relationship between state-independent flipping rates ($w_{s,F_1[s]}$, $w_{s,F_{12}[s]}$) and their corresponding quantum parameters (h_1^x, J_{12}^{xx}) in a 2-spin homogenous system.

The left plot shows a parameter sweep over all transitions involving spin 1 flipping (w_{13} and $w24$) in a non-interacting system ($J_{12} = 0$, $h_2 = 0$) with the other off-diagonal entries of the transition matrix made arbitrarily small $w_{s,F_2[s]} = 20$, $w_{s,F_{12}[s]} = 20$. We observe that the only quantum parameter affected in response to this sweep is h_1^x.

The right plot shows a sweep over all transitions involving spin 1 and 2 flipping (w_{14} and $w23$) in a non-interacting system ($J_{12} = 0$, $h_2 = 0$) with the other off-diagonal entries of the transition matrix made arbitrarily small $w_{s,F_1[s]} = 20$, $w_{s,F_2[s]} = 20$. In this case, we observe that the only quantum parameter affected by the parameter sweep is J_{12}^{xx}.

When performing the inverse mapping, in which a quantum Hamiltonian containing only h_1^x or J_{12}^{xx} is mapped to a transition matrix, we observe that increasing h_1^x results in an increased flipping rate for spin 1, while increasing J_{12}^{xx} leads to an increased flipping rate for both spin 1 and spin 2.

Based on these findings, we conclude that the b_i^0 term in our transition rate parametrization is directly proportional to h_1^x and that the b_{ij}^0 term is directly proportional to J_{ij}^{xx}.

5.3 State-dependent flipping rates

The expressions given by (2.17) and (2.16) also contain state-dependent transition terms:

1. b_k: A term that depends on a non-transitioning spin s_k.
2. b_{ij}: A term that depends on the product $s_i s_j$ of the spins s_i and s_j being flipped,
3. b_{kl}: A term that depends on the product of non-transitioning spins $s_k s_l$.

In this section, we search for quantum parameters that correspond to these terms. In the following sections, we try to establish a connection between these terms and the quantum parameters.

Non-transitioning spin dependence

When using a QBM with a model Hamiltonian as defined in Equation (3.8), we can calculate the matrix elements corresponding to single spin flips of the 2-qubit Hamiltonian as follows:

$$\langle s|\hat{H}|F_i[s]\rangle = \left(h_i^x - \sum_{j=1}^{n} J_{ij}^{xz} s_j\right) \tag{5.1}$$

Where we did not include the h_i^y term because $\hat{\rho}$ should be real-valued. This expression suggests a correspondence between b_k and J^{xz}. To analyse this correspondence, we want to isolate the effect of the b_k term. For a 2-spin system, we can adapt equation (2.16) as follows:

$$w_{s,F_1[s]}(s_2) = b_1^0 + b_2 s_2$$

If we then vary the hyperparameter $H_1 = w_{s,F_1[s]}(s_2 = 1) - w_{s,F_1[s]}(s_2 = -1)$, or equivalently $H_1 = w_{13} - w_{24}$ we see that any dependence on b_1^0 drops out.

Figure 5.3 shows the relationship between state-dependent transition rates $w_{s,F_1[s]}(s_2)$ and the corresponding quantum parameters (h_1^x, J_{12}^{xz}, h_2^z) in a 2-spin system homogenous system. In the plot, w_{24} $[(01) \to (11)]$ is increased while w_{13} $[(00) \to (10)]$ is decreased by the same amount. The x-axis indicates the magnitude of this change, with the middle of the plot corresponding to $w_{13} = w_{24} = 4$. The system considered is non-interacting ($J_{12} = 0$, $h_i = 0$). Any transition rates that are not part of the parameter sweep are set to $w_{s,s'} = 20$, which ensures the corresponding transition is very unlikely, so we can focus on the effects being investigated.

We can conclude that when we make the transitions involving the flipping of s_1 depend on the state $s_2 = \pm 1$, we observe the emergence of three quantum parameters: h_1^x, h_2^z and J_{12}^{xz}. Interestingly, the effects of J_{12}^{xz} and h_2^z cancel each other out for all values during the parameter sweep.

We can identify two distinct regimes. In the small-scale regime, changes in the hyperparameter H_1 lead to linear responses in J_{12}^{xz} and h_2^z, while h_1^x remains relatively stable. In the large-scale regime, all three parameters respond equally to variations in H_1. These results have been derived analytically, and you can find further details in Appendix B.

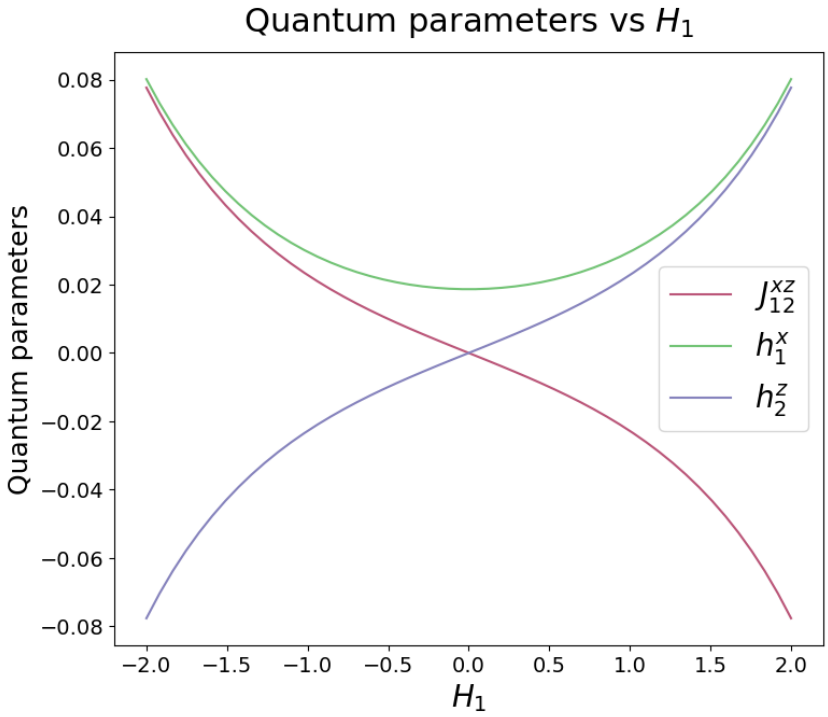

FIGURE 5.3: Relationship between the hyperparameter H_1 and the corresponding quantum parameters in a 2-spin homogenous system. The plot shows a forward mapping parameter sweep over $H_1 = w_{13} - w_{24}$. The x-axis represents the increase in w_{13} and the decrease in w_{24}, where the middle of the plot corresponds to $w_{13} = w_{24} = 4$. The system is non-interacting ($J_{12} = 0$) and without biases ($h_i = 0$). Transition rates that are not part of the sweep are set to $w_{s,s'} = 20$.

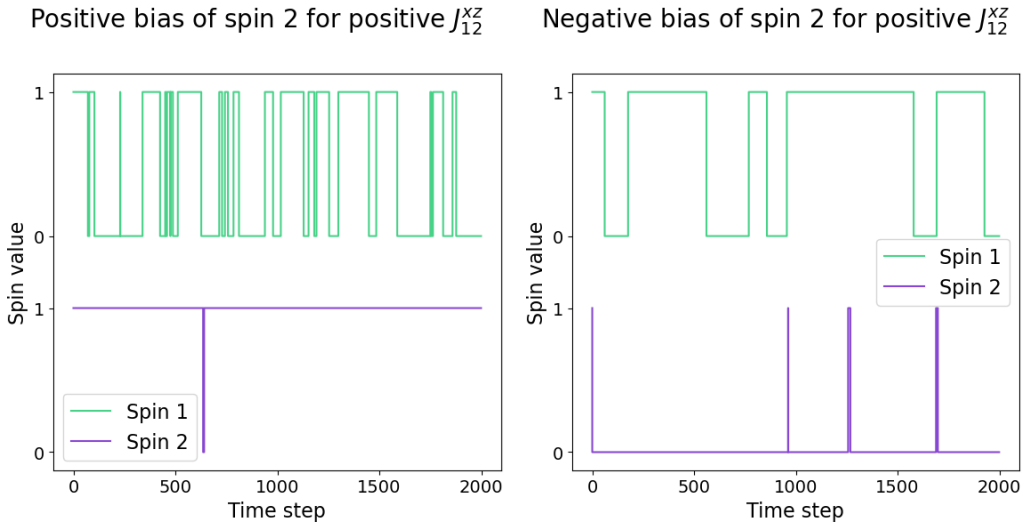

FIGURE 5.4: Evolution of the individual spins s_1 and s_2 for a quantum Hamiltonian with a positive $J_{12}^{xz} = 0.007$ for different values h_2^z. In both plots, single flip rates $h_1^x = 0.01$ and $h_2^x = 0.01$ were used to obtain a positive density matrix. Left: h_2^z = 0.05. The observed flipping rate of s_1 is higher compared to the same dynamics with $J_{12}^{xz} = 0$. Right: h_2^z = -0.05. The flipping rate is lower compared to the same dynamics with $J_{12}^{xz} = 0$.

Figure 5.4 shows the inverse mapping of a quantum Hamiltonian with a positive $J_{12}^{xz} = 0.007$ for different values ofh_2^z. In both plots, single flip rates $h_1^x = 0.01$ and $h_2^x = 0.01$ were used to obtain a positive density matrix. The other quantum parameters are all set to zero. The left plot shows the dynamics for a positive h_2^z and the right plot shows the dynamics for a negative h_2^z, both for a positive $J_{12}^{xz} = 0.007$.

The plots demonstrate that if we have a non-zero J_{12}^{xz} term, the dynamics has single flip transition rates s_1 that depend on the state $s_2 = \pm 1$. For a constant $J_{12}^{xz} = \pm c$ value, there is an increase in the flipping rate of s_1 when $s_2 = \pm 1$ and a decrease in flipping rate when $s_2 = \mp 1$.

Similar results can be observed for the J_{12}^{zx} term, with the role of spin 1 and spin 2 reversed. The described results also generalize to 3-spin systems, where for example J_{13}^{xz} encodes the dependence of the flip rate of s_1 on the state of $s_3 = \pm 1$.

Transitioning spin product dependence

The matrix elements corresponding to double spin flips of the 2-qubit Hamiltonian as given by:

$$\langle s|\hat{H}|F_{ij}[s]\rangle = \left(J_{ij}^{x} - J_{ij}^{yy} s_i s_j\right) \tag{5.2}$$

This expression suggests a correspondence between b_{ij} and J_{ij}^{yy}. To analyse this correspondence, we want to isolate the effect of the b_{ij} term. For a 2-spin system, we can adapt equation (2.17) as follows:

$$w_{s,F_{12}[s](s_2)} = b_{12}^0 + b_{12} s_1 s_2$$

If we then vary the hyperparameter $H_2 = w_{s,F_{12}[s]}(s_1 s_2 = 1) - w_{s,F_{12}[s]}(s_1 s_2 = -1)$, or equivalently $H_2 = w_{14} - w_{23}$ we see that any dependence on b_{12}^0 drops out.

Figure 5.5 shows the relationship between state-dependent transition rates $w_{s,F_{12}[s]}(s_1 s_2)$ and the corresponding quantum parameters (J_{12}^{xx}, J_{12}^{yy}, J_{12}^{zz}) in a 2-spin system homogenous system. In the plot, w_{14} $[(00) \rightarrow (11)]$ is increased while w_{23} $[(01) \rightarrow (10)]$ is decreased by the same amount. The x-axis indicates the magnitude of this change, with the middle of the plot corresponding to $w_{14} = w_{23} = 4$. The system considered is non-interacting ($J_{12} = 0$, $h_i = 0$). Any transition rates that are not part of the parameter sweep are set to $w_{s,s'} = 20$.

We can conclude that when we make the transitions involving the flipping of s_1 and s_2 depend on the product $s_1 s_2 = \pm 1$, we observe the emergence of three quantum parameters: J_{12}^{xx}, J_{12}^{yy}, and J_{12}^{zz}. Interestingly, the parameters J_{12}^{yy} and J_{12}^{zz} are equal to each other for all values during the parameter sweep.

We can identify two distinct regimes. In the small-scale regime, changes in the hyperparameter H_2 lead to linear responses in J_{12}^{yy} and J_{12}^{zz}, while J_{12}^{xx} remains relatively stable. In the large-scale regime, all three parameters respond equally to variations in H_2.

Figure 5.6 shows the evolution through state space of the combined system $s = (s_1, s_2)$ for a quantum Hamiltonian with a positive $J_{12}^{yy} = 0.007$ for different values of h_2^z. In both plots, double flip rates $J_{12}^{xx} = 0.008$ are used to obtain a positive density matrix. The other quantum parameters were all set to zero. The left plot shows the double flip rate, starting in an 'even' state where $s_1 s_2 = 1$ for a positive

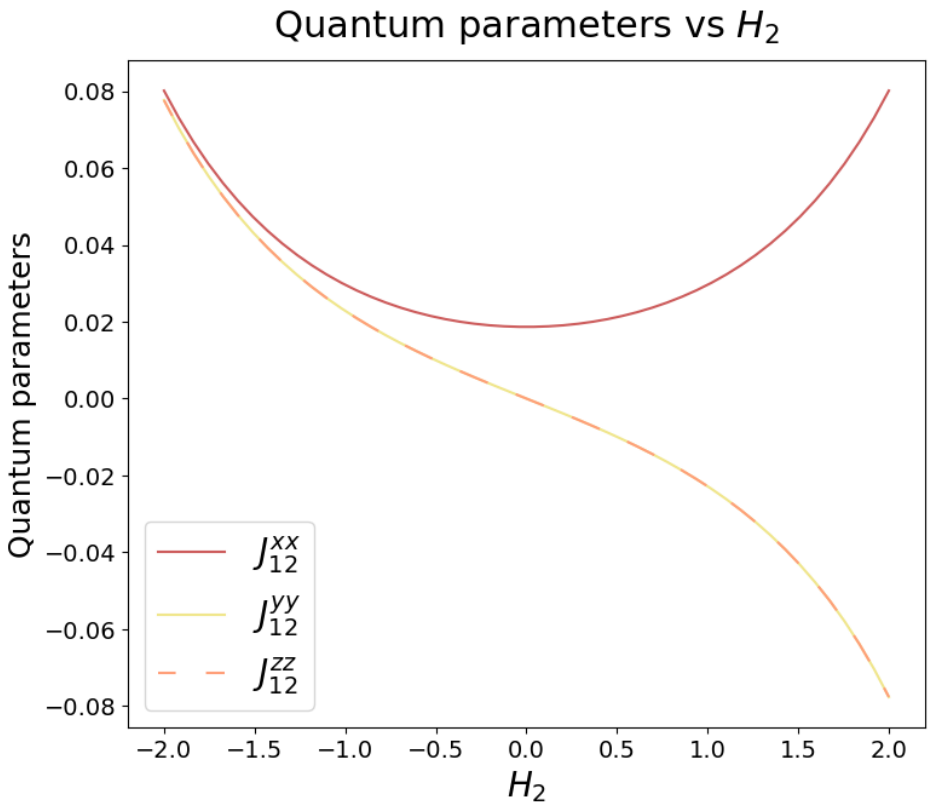

FIGURE 5.5: Relationship between the hyperparameter H_2 and the corresponding quantum parameters in a 2-spin homogenous system. The plot shows a forward mapping parameter sweep over $H_2 = w_{14} - w_{23}$. The x-axis represents the increase in w_{14} and the decrease in w_{23}, where the middle of the plot corresponds to $w_{14} = w_{23} = 4$. The system is non-interacting ($J_{12} = 0$) and without biases ($h_i = 0$). Transition rates that are not part of the sweep are set to $w_{s,s'} = 20$.

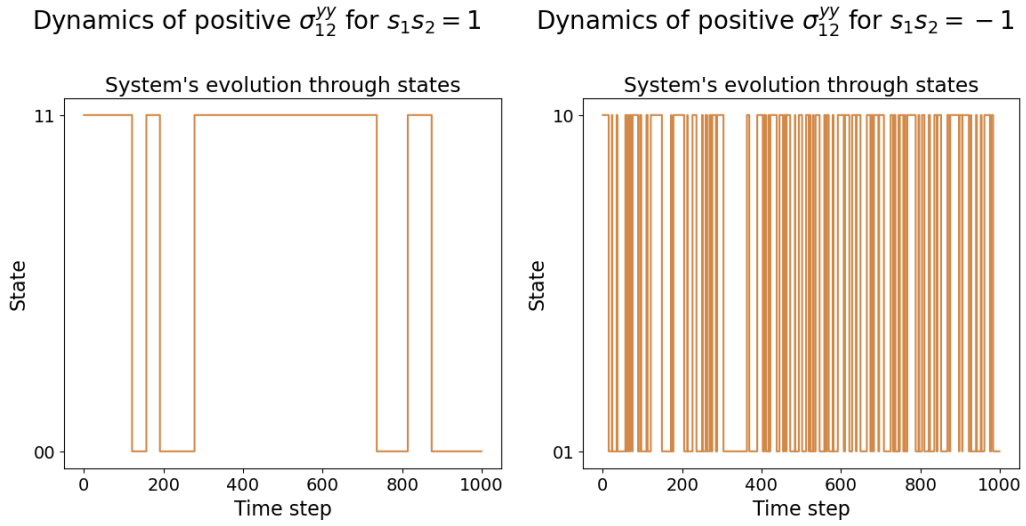

FIGURE 5.6: Evolution through state space of the combined system $s = (s_1, s_2)$ for a quantum Hamiltonian with a positive $J_{12}^{yy} = 0.007$ for different values of h_2^z. In both plots, double flip rates $J_{12}^{xx} = 0.008$ are used to obtain a positive density matrix. Left: Transition rate of w_{14} with $s_i s_j = 1$ for a constant J_{12}^{yy}. The observed flipping rate is higher compared to the same dynamics with $J_{12}^{yy} = 0$. Right: Transition rate of w_{23} with $s_i s_j = -1$. The observed flipping rate is lower compared to the same dynamics with $J_{12}^{yy} = 0$.

J_{12}^{yy}. The right plot shows the double flip rate, starting in an 'odd' state where $s_1 s_2 = -1$ for a positive J_{12}^{yy}.

This plot demonstrates that if we have a non-zero J_{12}^{yy} term, the dynamics has double flip transition rates of s_1 and s_2 that depend on the product $s_1 s_2 = \pm 1$. For a constant $J_{12}^{yy} = \pm c$ value, the double flip rate of s_1 and s_2 of the transition with $s_1 s_2 = \mp 1$ is increased while the rate of the transition with $s_1 s_2 = \pm 1$ is decreased.

Similar results as described above were obtained for the J_{1234}^{yyyy} term, but not included. J_{ijkl}^{YYYY} encodes that the quadruple flip rate of s_i,s_j,s_k and s_l depends on the product $s_i s_j s_k s_l$. The described results also generalize to 3-spin systems, where for example J_{13}^{yy} encodes the dependence of the double-spin flip rate of s_1 and s_3 on the product of $s_1 s_3 = \pm 1$. These findings appear to be in line with our explanation thus far.

Non-transitioning spin product dependence

$$\langle s|\hat{H}|F_i[s]\rangle = \left(h_i^x - \sum_j^n J_{ij}^{xz} s_j + \sum_{\langle k,l \rangle} \sigma_{ikl}^{xzz} s_k s_l \right) \tag{5.3}$$

Where $\langle k, l \rangle$ indicates summation over pairs $k, l \neq i$ and the h_i^y term is neglected because $\hat{\rho}$ should be real-valued. This expression suggests a correspondence between b_{kl} and σ_{ikl}^{xzz}. To analyse this correspondence, we want to isolate the effect of the b_{kl} term. For a 3-spin system, we can adapt equation (2.16) as follows:

$$w_{s,F_1[s](s_2)} = b_1^0 + b_2 s_2 + b_3 s_3 + b_{23} s_2 s_3$$

If we then vary the hyperparameter $H_3 = w_{s,F_1[s]}(s_2 s_3 = 1) - w_{s,F_1[s]}(s_2 s_3 = -1)$, or equivalently $H_3 = (w_{15} + w_{48}) - (w_{26} + w_{37})$ we see that any dependence on b_{12}^0, b_2 and b_3 drops out.

Figure 5.7 shows the relationship between state-dependent transition rates $w_{s,F_1[s]}(s_2 s_3)$ and the corresponding quantum parameters (h_1^x, J_{23}^{zz}, σ_{123}^{xzz}) in a 3-spin system homogenous system.

In the plot, w_{15} $[(000) \rightarrow (100)]$ and w_{48} $[(011) \rightarrow (111)]$ are increased while $w_{26} = 4$ $[(001) \rightarrow (101)]$ and $w_{37} = 4$ $[(010) \rightarrow (110)]$ are decreased by the same amount. The x-axis indicates the magnitude of this change, with the middle of the plot corresponding to $w_{15} = w_{48} = w_{26} = w_{37} = 4$. The system considered is non-interacting ($J_{ij} = 0$, $h_i = 0$). Any transition rates that are not part of the parameter sweep are set to $w_{s,s'} = 20$.

We can conclude that when we make the transitions involving the flipping of s_1 depend on the product $s_2 s_3 = \pm 1$, we observe the emergence of three quantum parameters: h_1^x, J_{23}^{zz}, and σ_{123}^{xzz}. The parameters h_1^x and σ_{123}^{xzz} are equal to each other for all values during the parameter sweep.

We can identify two distinct regimes. In the small-scale regime, changes in the hyperparameter H_3 lead to linear responses in J_{23}^{zz} and σ_{123}^{xzz}, while h_1^x remains relatively stable. In the large-scale regime, all three parameters respond equally to variations in H_3.

Figure 5.8 shows the evolution through state space of the combined system $s = (s_1, s_2, s_3)$ for a quantum Hamiltonian with a positive $\sigma_{123}^{xzz} = \pm 0.007$ for different

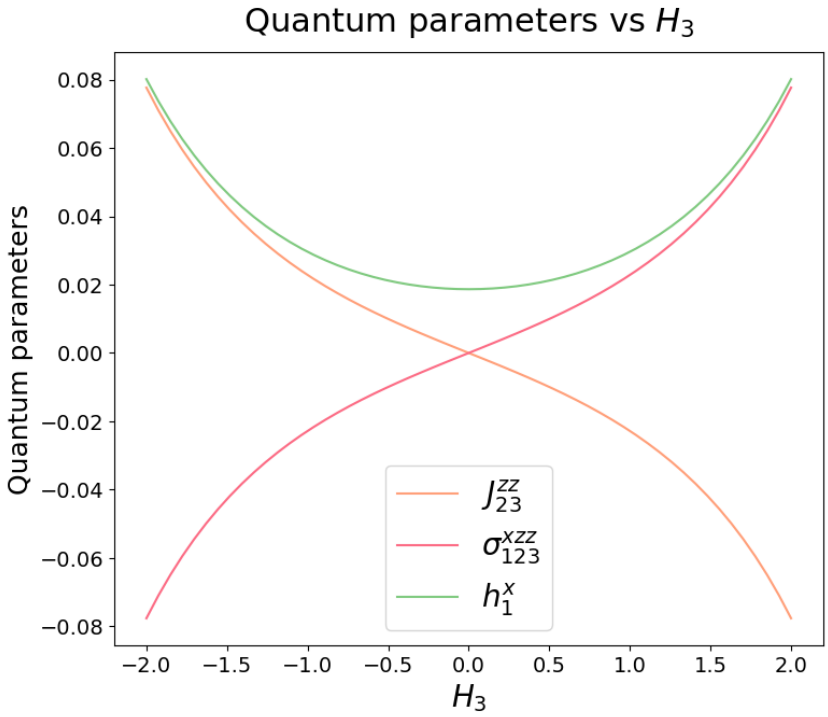

FIGURE 5.7: Relationship between the hyperparameter H_3 and the corresponding quantum parameters in a 3-spin homogenous system. The plot shows a forward mapping parameter sweep over $H_3 = (w_{15} + w_{48}) - (w_{26} + w_{37})$. The x-axis represents the increase in w_{15} and w_{48} and the decrease in w_{26} and w_{37}, where the middle of the plot corresponds to $w_{15} = w_{48} = w_{26} = w_{37} = 4$. The system is non-interacting ($J_{ij} = 0$) and without biases ($h_i = 0$). Transition rates that are not part of the sweep are set to $w_{s,s'} = 20$.

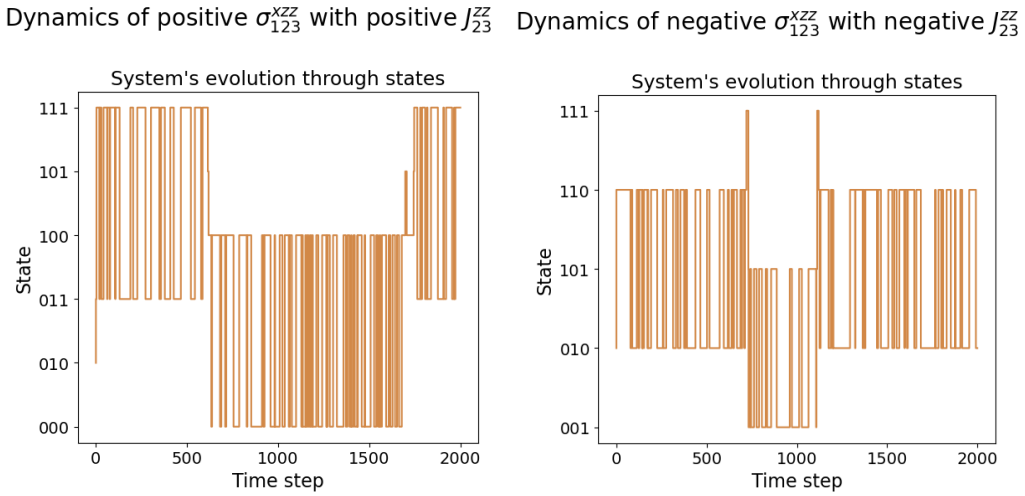

FIGURE 5.8: Evolution through state space of the combined system $s = (s_1, s_2, s_3)$ for a quantum Hamiltonian with a positive $\sigma_{123}^{xzz} = \pm 0.007$ for different values of J_{23}^{zz}. In both plots, single flip rates $h_1^x = 0.01$ are used to obtain a positive density matrix. Left: A $J_{23}^{zz} = 0.09$. The transitions rates w_{15} and w_{48} are significantly increased compared to when $J_{23}^{zz} = 0$. Right: A $J_{23}^{zz} = -0.09$. The transitions rates w_{26} and w_{37} are significantly increased compared to $J_{23}^{zz} = 0$.

values of J^{zz}_{23}. In both plots, single flip rates $h^x_1 = 0.01$ are used to obtain a positive density matrix. The other quantum parameters were all set to zero.

The left plot shows the dynamics for a positive $\sigma^{xzz}_{123} = 0.07$ and positive $J^{zz}_{23} = 0.09$. The right plot shows the dynamics for a negative $\sigma^{xzz}_{123} = -0.07$ and negative $J^{zz}_{23} = -0.09$. In both plots, there is a small single-spin flip applied to each spin using $h^x_i = 0.01$ to better visualize the effects and to obtain a positive density matrix from the quantum Hamiltonian. The other quantum parameters are all set to zero. The left plot shows the single flip rate, starting in an 'even' state where $s_2 s_3 = 1$ for a positive σ^{xzz}_{123}. The right plot shows the double flip rate, starting in an 'odd' state where $s_2 s_3 = -1$ for a negative σ^{xzz}_{123}.

This plot demonstrates that if we have a non-zero σ^{xzz}_{123} term, the dynamics has single-flip transition rates of s_1 that depend on the product $s_2 s_3 = \pm 1$. The single flip rate of s_1 of the transitions with $s_2 s_3 = \pm 1$ when $J^{zz}_{kl} = \pm 1$ and decreased when $J^{zz}_{kl} = \mp 1$. The described results also generalize to other terms, where for example σ^{zxz}_{123} encodes the dependence of the flipping rate of s_2 on the product $s_1 s_3 = \pm 1$.

6 Conclusion & Discussion

In conclusion, our findings demonstrate that the parameters of a QBM encode both equilibrium and dynamical properties of a binary stochastic dynamics. We established direct relations for the classical equilibrium parameters h_i and J_{ij} to the quantum parameters h_i^z and J_{12}^{zz}, respectively. Further, we established a direct relation between state-independent transitions rates $w_{s,F_i[s]}$ and $w_{s,F_{ij}[s]}$ and the quantum parameters h_i^x and J_{12}^{xx}.

Regarding state-dependent transition rates, we have established the following connections to the quantum parameters:

- J_{ij}^{xz} is linked to the single-spin flip rate of s_i depending on s_j.
- J_{ij}^{yy} is linked to the double-spin flip rate of s_i and s_j depending on the product $s_i s_j$.
- σ_{ijk}^{xzz} is linked to the single-spin flip rate of s_i depends on the product $s_j s_k$.

By varying the hyperparameter H, we have observed two distinct regimes that exhibit different qualitative behaviors for these parameters. In the small-scale regime, the state-dependent parameter and its associated z-parameter (h_i^z or J_{ij}^z) change linearly with H, while the associated x-parameter (h_i^x or J_{ij}^z) shows little response. In the large-scale regime, all three parameters respond equally.

Overall, we can understand classical dynamical properties as interactions in an equilibrium quantum model. This also demonstrates why the QBM can learn certain classical tasks better. It does not only have more parameters, but the parameters also encode more information than the BM has access to. We see that by quantizing this classical algorithm, we gain the ability to infer both state-dependent and state-independent dynamical effects.

For the state-dependent transition rates, we merely established links to quantum parameters. Due to other terms appearing in the quantum Hamiltonian together with the mentioned terms, we cannot assign a direct correspondence. However, it is possible to derive these relationships analytically, as demonstrated in Appendix B for the J_{ij}^{xz} term. The analytical derivations for the other terms are expected to follow a similar approach.

The systems the plots were generated for exhibited a high degree of symmetry. To this end, the found results can provide aid in deriving analytical solutions. The results also suggest certain combinations of quantum parameters might encode different properties. Further research on this is also required. Once the homogenous systems are well-understood with analytical derivations, it might be fruitful to analyse connected systems.

Looking ahead, the logical framework demonstrating how "mixed terms" encode state-dependent transitions can be extended to higher-order terms not included in the results. Some examples of these terms include:

- J_{ijk}^{xxz}, which is associated with the double flip rate of s_i and s_j depending on the spin k.
- J_{ijk}^{xyy}, which is linked to the triple-spin flip rate of s_i, s_j, and s_k based on the product $s_j s_k$.
- J_{ijkl}^{yyxz}, which is associated with the triple-spin flip rate of s_i, s_j, and s_k depending on the product $s_i s_j s_l$.

In general, within a mixed term, the symbol "x" indicates involvement in the transition without dependency on the value, "y" indicates involvement in the transition with dependency on the product of other "y" and "z" terms, and "z" indicated no involvement in the transition but dependency on the specified spin or, in the case of multiple "y" and "z" terms, dependency on the product of those terms.

Expanding on this logic, the term h_i^y would encode how the single-spin flip rate of s_i depends on its own value. If we allowed the flipping rates to depend on the spins being flipped, it would result in an asymmetric density matrix and non-detailed balance dynamics. This hints at a correspondence between the odd-y quantum parameters and non-DB dynamics. A potential way to test this hypothesis is described in Appendix C.

Acknowledgements

I would like to thank my daily supervisor Eduardo Domínguez Vázquez for his guidance, patience, and the lively discussions we had. I have gained a wealth of knowledge as a result of this research, which would not have been possible without him helping me to see both the big picture and its intricate details. I also would like to thank Prof. Dr. H.J. Kappen and Prof. Dr. A.C.C Coolen for their helpful comments and contributions. Exploring the connections between statistical mechanics, quantum physics, and machine learning has been a thought-provoking experience for which I am grateful.

A The Boltzmann Machine

The Boltzmann Machine (BM) is a statistical machine learning model based on the Boltzmann distribution of an Ising model. It represents data as a thermal state of an Ising model Hamiltonian [35]. A BM can be used to learn the parameters of a given Ising Hamiltonian that best describes an empirical data distribution $q(s)$.

A.1 The Ising Model

A general Ising model consists of a lattice of N binary spins $s = \{s_1, \ldots, s_N\}$ with $s_i = \pm 1$. The energy scalar associated with a state is given by the Hamiltonian equation:

$$H(s) = -\sum_{ij} J_{ij} s_i s_j - \sum_i h_i s_i \tag{A.1}$$

where J encodes the interaction strengths between the spins and h the local field interactions of the spins. The probability of a state s is given by the Boltzmann distribution:

$$p(s) = \frac{e^{-\beta H(s)}}{Z} \tag{A.2}$$

A.2 Boltzmann Machine Learning

The learning process of a BM involves adjusting the weights of the connections to capture the statistical dependencies in the observed data. This is done by maximizing the log-likelihood between the target distribution $q(s)$ and the model distribution $p(s)$ using gradient ascent. The log-likelihood function is given by [36]

$$L(w, h) = \frac{1}{P} \sum_{\mu} \log p(s^{\mu}) \tag{A.3}$$

with P training patterns $s = s^1, \ldots s^P$. Substituting the Boltzmann probabilities (A.2) in this equation, we can rewrite the equation in the form:

$$L(w, h) = \frac{1}{P} \sum_{\mu} -H(s^{\mu}) - \log Z \tag{A.4}$$

with $H(s^{\mu})$ being given by (A.1). The learning rules can be obtained by maximizing this equation with respect to the parameters (J, h):

$$J_{ij}^t = J_{ij}^{t-1} + \eta \frac{\delta L}{\delta J_{ij}} = J_{ij}^{t-1} + \eta(\langle s_i s_j \rangle_q - \langle s_i s_j \rangle_p) \tag{A.5}$$

and

$$h_i^t = h_i^{t-1} + \eta \frac{\delta L}{\delta h_i} = h_i^{t-1} + \eta(\langle s_i \rangle_q - \langle s_i \rangle_p) \tag{A.6}$$

We refer to $\langle s_i \rangle_q$ and $\langle s_i s_j \rangle_q$ as the clamped statistics and $\langle s_i \rangle_p$ and $\langle s_i s_j \rangle_p$ as the free statistics. The clamped statistics can be computed from the data. These update rules ensure that the observed data is the most probable under the Boltzmann distribution (A.2) with the learned parameters (J, h). Learning is terminated once the first and second-order statistics of the target and model distribution have converged within a certain threshold:

$$\langle s_i s_j \rangle_\rho = \langle s_i s_j \rangle_\eta \qquad \langle s_i \rangle_\rho = \langle s_i \rangle_\eta \tag{A.7}$$

The described learning process is summarized by the following algorithm:

Algorithm 2: Boltzmann Machine Learning Algorithm

Data: Input data set
Result: Trained Boltzmann Machine
Initialize the weights and biases of the Boltzmann machine;
Compute the expectation values and correlations from the data, store as P_{clamp};
while *the stopping criterion is not met* **do**
    Let the network reach thermal equilibrium;
    Compute the expectation values of the correlations, store as P_{free};
    Update the weights and biases based on the difference $P_{clamp} - P_{free}$;
end

B Analytical derivation of the XZ term

For a homogenous system ($J_{12} = 0$, $h_i = 0$) with only single spin flip transitions, we can express the single-flip rate using equations (2.8) and (2.16):

$$g_i(s) = \exp\left(b_i^0 + b_i s_j\right) \tag{B.1}$$

We can then write the transition matrix given by (2.7) as:

$$W(s'|s) = W(s', s)\delta_{s,s'} + \sum_i \exp\left(b_i^0 + b_i s_j\right) \delta_{s,F_i[s]}$$

To simplify further, we use the expansion:

$$e^{AS} = \cosh(A) + s\sinh(A)$$

This allows us to rewrite the transition matrix as:

$$W(s'|s) = W(s', s)\delta_{s,s'} + \sum_i (C_{ij} + D_{ij} s_j)\delta_{s,F_i s} \tag{B.2}$$

where

$$C_i \equiv \exp\left(b_i^0\right)\cosh(b_i)$$
$$D_i \equiv \exp\left(b_i^0\right)\sinh(b_i)$$

Expanding $W(s', s)$ using the definition $W(s', s) = 1 - \sum_s W(s'|s)$, we obtain:

$$W = \left(1 - \sum_i C_i\right)\delta_{s,s'} - \sum_i D_i s_j \delta_{s,F_j[s]} + \sum_i \left[C_i \delta_{s,F_i[s']} + D_i s_j \delta_{s,F_i[s']}\right] \tag{B.3}$$

Since the steady state of this system is constant, we can derive the density matrix directly from the transition matrix. Using that $\hat{\rho}(s', s) = cW(s', s)$, we can decompose W into quantum interaction terms:

$$\begin{aligned}
\langle s|\hat{I}|s'\rangle &= \delta_{s,s'} \\
\langle s|\hat{\sigma} i^z|s'\rangle &= s_i\langle s'|s\rangle = s_i \delta s, F_i[s] \\
\langle s|\hat{\sigma} i^x|s'\rangle &= \langle s|F_i[s']\rangle = \delta s, F_i[s] \\
\langle s|\hat{\sigma}_i^x \hat{\sigma}_j^z|s'\rangle &= s_j\langle s|\hat{\sigma} i^x|s'\rangle = s_j \delta s, F_i[s]
\end{aligned}$$

Combining these with the transition matrix (B.3), we arrive at the desired parametrization using quantum parameters:

$$W = \left(1 - \sum_i C_i\right)\hat{I} - \sum_i D_i \hat{\sigma}_j^z + \sum_i \left[C_i \hat{\sigma}_i^x + D_i \hat{\sigma}_i^x \hat{\sigma}_j^z\right] \tag{B.4}$$

From this, we observe that:

$$h_i^x = C_i$$
$$J_{ij}^{xz} = D_i$$
$$h_j^z = -D_i$$

These equations explain the relationship between J_{ij}^{xz} and h_j^z as shown in Figure. The parameters C_i and D_i also influence the shape of the curves in Figure 5.3, providing a mathematical explanation for the observed two distinct regimes.

C Non DB dynamics

In certain applications of binary stochastic neural networks, such as gene regulatory networks in neural networks, it is not realistic to assume symmetric connections between the binary variables [35]. As a result, the principle of detailed balance (DB) is generally not satisfied, and the dynamics may not reach an equilibrium distribution. Analysing these non-DB directly using a QBM is not possible, because the transition matrix associated with the system is not symmetric, and thus cannot be converted into a Hermitian density matrix using the procedure described in Chapter 4.

To address this, we propose decomposing the transition matrix into two parts: one that satisfies detailed balance (W_s) and one that does not (W_{as}), where $W = W_s + W_{as}$. For detailed balance to hold, the probability flux $F = W(s|s')p(s)$ should be symmetric. The decomposition of W can be done as follows:

$$\Pi = \text{diag}(p(s)) \; F \quad = \Pi W \; W = \Pi^{-1} F$$

We can further split the flux into symmetric and asymmetric parts:

$$F_s = \frac{F + F^T}{2} \; F_{as} \quad = \frac{F - F^T}{2}$$

Using these definitions, we can express the symmetric and antisymmetric transition matrices as:

$$W_s = \Pi^{-1} F_s \; W_{as} \quad = \Pi^{-1} F_{as}$$

It follows that:

$$W_s = \frac{W + \Pi W^T \Pi^{-1}}{2} \text{ where } F^T \quad = (W\Pi)^T = \Pi^T W^T = \Pi W^T$$

Hence, we have the decomposition:

$$W_{s/as} = \left[\frac{W \pm \Pi W^T \Pi^{-1}}{2} \right]$$

We can then convert W_s into a real symmetric density matrix $\hat{\rho}s$ and Was into an asymmetric density matrix $\hat{\rho}_{as}$. If we define the density matrix as $\hat{\rho} = \hat{\rho}s + i\hat{\rho}as$, we obtain a Hermitian density matrix that the QBM can learn. This allows us to explore the connection between the QBM's odd-Y quantum parameters and non-detailed balance dynamics.

Bibliography

[1] M. I. Jordan and T. M. Mitchell. "Machine learning: Trends, perspectives, and prospects". In: *Science* 349.6245 (2015), pp. 255–260. DOI: 10.1126/science.aaa8415.

[2] Martin Pichl, Eva Zangerle, and Günther Specht. "Understanding user-curated playlists on spotify: A machine learning approach". In: *International Journal of Multimedia Data Engineering and Management (IJMDEM)* 8.4 (2017), pp. 44–59.

[3] Qing Rao and Jelena Frtunikj. "Deep learning for self-driving cars: Chances and challenges". In: *Proceedings of the 1st international workshop on software engineering for AI in autonomous systems*. 2018, pp. 35–38.

[4] Myeongsuk Pak and Sanghoon Kim. "A review of deep learning in image recognition". In: *2017 4th international conference on computer applications and information processing technology (CAIPT)*. IEEE. 2017, pp. 1–3.

[5] Giuseppe Carleo et al. "Machine learning and the physical sciences". In: *Reviews of Modern Physics* 91.4 (2019), p. 045002.

[6] Urs Köster et al. "Higher order correlations within cortical layers dominate functional connectivity in microcolumns". In: *arXiv preprint arXiv:1301.0050* (2013).

[7] Frank Noé, Gianni De Fabritiis, and Cecilia Clementi. "Machine learning for protein folding and dynamics". In: *Current opinion in structural biology* 60 (2020), pp. 77–84.

[8] Karthik Kashinath et al. "Physics-informed machine learning: case studies for weather and climate modelling". In: *Philosophical Transactions of the Royal Society A* 379.2194 (2021), p. 20200093.

[9] Nathalie P de Leon et al. "Materials challenges and opportunities for quantum computing hardware". In: *Science* 372.6539 (2021), eabb2823.

[10] David Peral García, Juan Cruz-Benito, and Francisco José García-Peñalvo. "Systematic literature review: Quantum machine learning and its applications". In: *arXiv preprint arXiv:2201.04093* (2022).

[11] Amine Zeguendry, Zahi Jarir, and Mohamed Quafafou. "Quantum Machine Learning: A Review and Case Studies". In: *Entropy* 25.2 (2023), p. 287.

[12] H Ij. "Statistics versus machine learning". In: *Nat Methods* 15.4 (2018), p. 233.

[13] Mária kieferová and Nathan Wiebe. "Tomography and generative training with quantum Boltzmann machines". In: *Physical Review A* 96.6 (2017). PRA, p. 062327. DOI: 10.1103/PhysRevA.96.062327.

[14] Nobuyuki Yoshioka, Yutaka Akagi, and Hosho Katsura. "Transforming generalized Ising models into Boltzmann machines". In: *Physical Review E* 99.3 (2019), p. 032113.

[15] Yann LeCun, Yoshua Bengio, and Geoffrey Hinton. "Deep learning". In: *nature* 521.7553 (2015), pp. 436–444.

[16] Ruslan Salakhutdinov and Geoffrey Hinton. "Deep Boltzmann machines". In: *Artificial intelligence and statistics*. PMLR. 2009, pp. 448–455.

[17] Geoffrey E Hinton, Simon Osindero, and Yee-Whye Teh. "A fast learning algorithm for deep belief nets". In: *Neural computation* 18.7 (2006), pp. 1527–1554. ISSN: 0899-7667.

[18] Terrence J Sejnowski. "Higher-order Boltzmann machines". In: *AIP Conference Proceedings*. Vol. 151. 1. American Institute of Physics. 1986, pp. 398–403.

[19] Mohammad H Amin et al. "Quantum Boltzmann machine". In: *Physical Review X* 8.2 (2018), p. 021050.

[20] H. J. Kappen. "Learning quantum models from quantum or classical data". In: *Journal of Physics A: Mathematical and Theoretical*. 53.21 (2020). ISSN: 1751-8113 1751-8121. DOI: 10.1088/1751-8121/ab7df6.

[21] Mark EJ Newman and Gerard T Barkema. *Monte Carlo methods in statistical physics*. Clarendon Press, 1999. ISBN: 0191589861.

[22] Wulfram Gerstner et al. *Neuronal dynamics: From single neurons to networks and models of cognition*. Cambridge University Press, 2014.

[23] Brian Kiraly et al. "An atomic Boltzmann machine capable of self-adaption". In: *Nature Nanotechnology* 16.4 (2021), pp. 414–420.

[24] Gabriel Fonseca Guerra. "Stochastic processes for neuromorphic hardware". PhD thesis. University of Manchester, 2020.

[25] Danijela Marković et al. "Physics for neuromorphic computing". In: *Nature Reviews Physics* 2.9 (2020), pp. 499–510. ISSN: 2522-5820. DOI: 10.1038/s42254-020-0208-2.

[26] André Longtin, Adi Bulsara, and Frank Moss. "Time-interval sequences in bistable systems and the noise-induced transmission of information by sensory neurons". In: *Physical review letters* 67.5 (1991), p. 656.

[27] David Ruelle. *Thermodynamic formalism: the mathematical structure of equilibrium statistical mechanics*. Cambridge University Press, 2004.

[28] JGraph. *diagrams.net*. Oct. 2021. URL: https://www.diagrams.net/.

[29] Anthony CC Coolen, Reimer Kühn, and Peter Sollich. *Theory of neural information processing systems*. OUP Oxford, 2005. ISBN: 0191583006.

[30] Christophe Andrieu et al. "An introduction to MCMC for machine learning". In: *Machine learning* 50 (2003), pp. 5–43.

[31] James R Norris. *Markov chains*. 2. Cambridge university press, 1998.

[32] Roy J Glauber. "Time-dependent statistics of the Ising model". In: *Journal of mathematical physics* 4.2 (1963), pp. 294–307.

[33] Onno Huijgen et al. "Training Quantum Boltzmann Machines with the β-Variational Quantum Eigensolver". In: *arXiv preprint arXiv:2304.08631* (2023).

[34] J. Pieterse. *QBM-code*. 2023. URL: https://github.com/ringo333/QBM-code.

[35] H Chau Nguyen, Riccardo Zecchina, and Johannes Berg. "Inverse statistical problems: from the inverse Ising problem to data science". In: *Advances in Physics* 66.3 (2017), pp. 197–261. ISSN: 0001-8732.

[36] David JC mackay and David JC Mac Kay. *Information theory, inference and learning algorithms*. Cambridge university press, 2003. ISBN: 0521642981.